Ice Sheet Observations Provide Economic Value of Information For Coastal Flood Risk Management

Abstract

Designing a strategy to manage future coastal flood risks requires information about the key uncertainties. One important uncertainty is the vulnerability of the West Antarctic Ice Sheet to global warming and the resulting sea-level changes. Here we expand on a classic flood defense model to quantify how accounting for ice-sheet observations can improve the reliability, investment costs, and expected damages compared to strategies which only use local sea level information. The economic value of this information increases with increased emissions scenarios due to the higher likelihood of accelerated ice sheet melting. The analysis suggests that ice sheet observations can serve as useful signposts for adaptive coastal flood-defense strategies.

1 Introduction

Future coastal flood risk is dependent on multiple deep uncertainties[1–5]. Deep uncertainties occur when there is no consensus among experts about the underlying probability distributions[6,7]. One key deep uncertainty is the future ice-sheet contribution to sea-level rise[1,2,8]. Some of the uncertainties driving future ice-sheet melting rates include emissions and melting dynamics[9–11]. Accelerating ice-sheet melting could increase mean global sea levels in 2100 by over a meter[12].

Observations of accelerated ice-sheet mass loss (for example, using remote sensing platforms such a GRACE[13]) could provide an early warning signal that coastal flood risk management strategies need to account for a higher rate of sea-level rise. Sudden changes to ice-sheet dynamics might hence serve as an important signpost to trigger adaptations in flood risk management strategies.

Here, we examine the economic value of the observing ice sheets for local decision-making about dike heightening by building on the decision framework used by Garner & Keller[14]. We consider strategies which explicitly consider global information about the ice-sheet contribution to sea-level rise. We demonstrate and quantify how these strategies can outperform strategies which only use local information with respect to economic and reliability objectives.

2 Methods

2.1 Underlying Flood-Risk Management Model

We use a modified version of the classic Eijgenraam flood risk management model[15]. The Eijgenraam model was designed to inform the timings and extents of levee heightenings in the Netherlands. The assumptions of the model (shared with the early van Dantzig model[16]) are that each levee ring floods only when the levee is overtopped and that the social costs (damages) associated with a flooding event is the entire value within the affected polder. While the original analysis by Eijgenraam et al[15] was for multiple dike rings, we focus on a single representative ring. We run the model from the years 2017 ($t = 0$) through 2100.

The optimization objective is to find a time series of annual levee heightenings u_t which minimizes the total discounted social cost,

$$\min_u \sum_t I(h_t^-, u_t)e^{-\delta t} + S_t e^{-\delta_1 t}, \tag{1}$$

where $I(h_t^-, u_t)$ is the investment cost to add height u_t to a levee with previous height h_t^- at time t, S_t is the expected damages at time t, and δ and δ_1 are discount rates (which allows the net present value of investments and damages to respond to different types of change). The investment cost function is exponential with respect to the previous levee height as well as the heightening amount[15,17],

$$I(h_t^-, u_t) = \begin{cases} 0 & u_t = 0 \\ (\kappa + v u_t) e^{\lambda(h_t^- + u_t)} & u_t > 0, \end{cases} \tag{2}$$

where κ, v, and λ are positive constants. The expected damages associated with flooding at time t are approximated by

$$S_t = P_t V_t, \tag{3}$$

where P_t is the probability of flooding at time t. The damages associated with a flood at time t, V_t, is given by

$$V_t = V_0^- e^{\gamma t} e^{\xi(h_t - h_0^-)},$$

where V_0^- are the base damages associated with a flood prior to $t = 0$, h_0^- is the initial levee height prior to $t = 0$, γ is the economic growth rate of the protected area, and ξ is the rate of loss increase per unit of levee heightening. The values of constants in this study are given in Table 1; they mostly correspond to the values for levee ring 16 (Alblasserwaard)[17] (aside from the initial levee height h_0^-, which was set to provide protection within the desired 1/2000 protection standard at $t = 0$, and the discount rates, which represent a base risk-free rate of 4% rather than the 2.5% used by Eijgenraam et al[17], as well as a risk premium of 1.5% for damages).

Table 1: Parameter values for the economic component of the base adaptation model described in Section 2.1

Parameter (symbol)	**Value**	**Unit**
Investment discount rate (δ)	0.04	yr^{-1}
Damages discount rate (δ_1)	0.055	yr^{-1}
Fixed levee heightening cost (κ)	324.6287	millions €
Investment cost linear rate (υ)	2.1304	€/cm
Investment cost exponential rate (λ)	0.01	cm^{-1}
Economic growth rate (γ)	0.025	yr^{-1}
Loss increase rate (ξ)	0.002032	cm^{-1}
Initial levee height, relative to 2000 mean sea level (h_0^-)	4500	cm
Initial loss due to flooding (V_0^-)	22656.5	€

2.2 Sea-Level Rise and Storm Surge Models

We use an ensemble of simulated future annual maximal water levels to determine the probability of flooding in each year. Projected changes to global mean sea levels are generated using the BRICK model[18]. These projections correspond to a mixture of temperature scenarios resulting from forcings equally distributed between RCPs 2.6, 4.5, 6.0, and 8.5 (see Figure S1). The global sea-level change projections are then transformed into absolute local mean sea-level projections at the Delfzijl tide-gauge station. We obtain relative local mean sea-level series by combining these absolute series with subsidence projections, assuming a linear subsidence rate of $0.76\,\mathrm{cm\,yr}^{-1}$[17].

We use a non-stationary generalized extreme value (GEV) distribution[19] to model the annual maximum deviation from the annual mean sea level. GEV distributions are characterized by three parameters (location, μ; scale,

σ; and shape, ξ). We assume that the location parameter has a linear dependence on global mean temperature T, so that $\mu = \mu_0 + \mu_1 T$[5,20]. We calibrate this storm-surge model using Markov Chain Monte Carlo and data from the Delfzijl tide gauge station[21] (see Table S1 for the prior distributions, and Figure S2 for the posterior distribution).

We produce annual maximal sea-level series, each corresponding to an individual state of the world (SOW), by combining a local relative mean sea-level series with residuals distributed according to a sampled GEV distribution. The non-stationary behavior of each GEV is determined by the BRICK-projected temperature series associated with the mean sea-level series. This process (along with the calculation of heightening policy levers described in Section 2.3) is illustrated in Figure 1. We sample 50,000 sea-level rise trajectories and surge distributions; a pair of a sea-level rise trajectory and surge distribution forms an SOW.

The potential modulation of water-level extremes by global climate variables has been the subject of active research[5,22,23]. For simplicity, we use a statistical dependence to reflect an aggregation of multiple mechanisms which influence maximum water levels and may be correlated with changes in temperature (such as increased bathymetric depth or potential changes in the frequency and intensity of storms). We quantify the relative ability of a temperature-dependent non-stationary GEV model to predict annual maximum water-level deviations from the mean at Delfzijl using the Watanabe-Akaike Information Criterion (WAIC)[24,25]. Like other information criteria

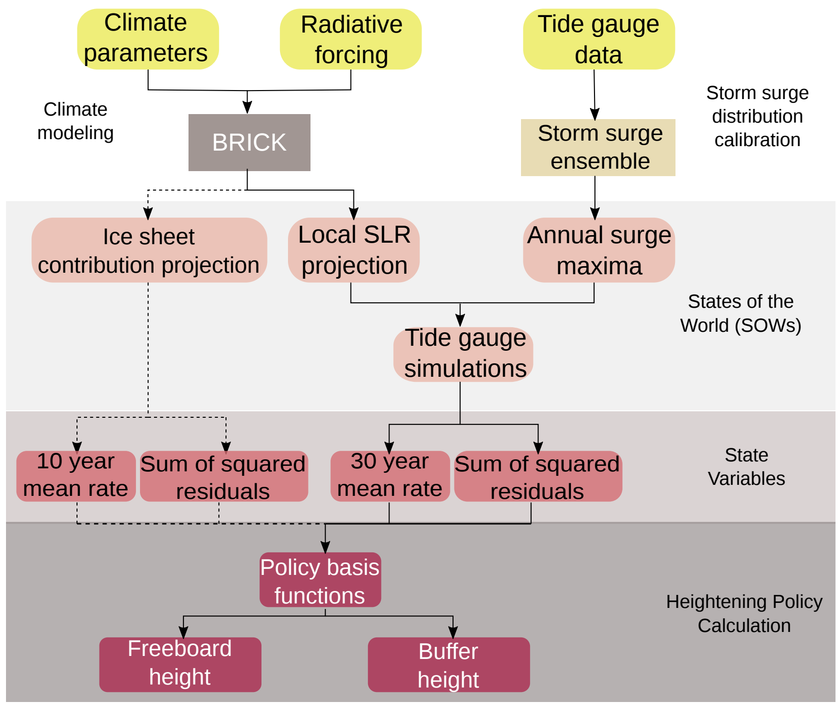

Figure 1: Model flowchart illustrating the information flow from sea-level rise and storm-surge ensemble generation to the heightening policy calculation.

such as the Akaike Information Criterion[26] and the Bayesian Information Criterion[27], lower AIC values suggest a better model fit. Using WAIC, the non-stationary model (modulated by global mean temperature), with a WAIC value of 2090, is the preferred model structure, as the stationary model has a WAIC value of 2106.

2.3 Policy Levers and Decision Variables

The original Eijgenraam model[15] produces a time series of levee heightenings, to be applied for all future realizations of flood risk. This approach can provide valuable insights, but it is silent on the possible benefits of learning. In other words, the original model is non-adaptive (the generated heightening series does not change in response to new observations) and requires a large number of decision variables (one for each model year). We will subsequently reference as the "local information" and "global information" strategies.

For both strategies, levee heightenings are prompted when the annual maximum water level comes within a particular buffer height from the top of the levee, suggesting that the levee could be overtopped in the future. The levee is then heightened to restore the buffer over the observed extreme water level and then further by a "freeboard" height, which allows for a certain amount of sea-level rise and surge intensification without requiring another building event. The buffer and freeboard heights are the policy levers. Heightening policies found using this buffer and freeboard formulation of the Eijgenraam model result in fewer damages at lower investment costs than the intertemporal formulation[14].

To allow these levers to dynamically respond to the observed SOW, we adopt a direct policy search (DPS)[14,28–30] formulation. In DPS, the decision policy levers are constructed from a set of basis functions defined over system states.

Both the local and global information strategies incorporate locally observed maximum water levels (y_t). State information about extreme water heights can serve as an important information source for heightening[31]. The first associated state variable we use is the observed mean rate of extreme water level increase β_t, which is obtained using a linear regression over a 30-year moving window of observations. Specifically, for $i = 0, \ldots, 29$, fitted values $\hat{y}_i$ are obtained as

$$\hat{y}_i = \alpha_t^{loc} + \beta_t^{loc} i.$$

The other local state variable is the square root of the sum of square residuals $srss_t$ over that window,

$$srss_t^{loc} = \sqrt{\sum_{i=t-30}^{t-1} (\hat{y}_i - y_i)^2}.$$

β_t^{loc} and $srss_t^{loc}$ describe the anticipated amount of future increases in extreme water levels and the observed variation around that trend, which provides a measure of volatility.

The second set of state variables adds information about the ice sheet contribution to global sea level rise to the local state variables β_t and $srss_t$. For each SOW, BRICK produces an annual series of Antarctic and Greenland ice sheet contributions in meters sea-level equivalent. The mean rate (via linear regression) and sum of squared residuals of the ice sheet series (β_t^{ice} and $srss_t^{ice}$, respectively) over a 10-year moving window are included along with the local state variables. We use a 10-year moving window for these global variables to increase sensitivity to changing ice-sheet melt rates, which can accelerate quickly under the right conditions[10], while a longer window for the local extreme observations helps smooth out the impact of short-term volatility.

We calculate the buffer and freeboard heights (BH and FH, respectively) using quadratic functions of the state variables. The choice of quadratic basis functions was selected for consistency with the previous work by Garner & Keller[14], where this formulation (using local observations) was found to outperform the original intertemporal formulation of the Eijgenraam model. For a local information policy, the heightening levers are obtained as

$$BH_t^{loc} = x_1 + x_2\beta_t^{loc} + x_3(\beta_t^{loc})^2 + x_4 srss_t^{loc} + x_5(srss_t^{loc})^2,$$
$$FH_t^{loc} = x_6 + x_7\beta_t^{loc} + x_8(\beta_t^{loc})^2 + x_9 srss_t^{loc} + x_{10}(srss_t^{loc})^2,$$

where the x_j are coefficients for the state variables, obtained through the optimization procedure outlined in Section 2.5 with respect to the objectives in Section 2.4. These coefficient values are a combination of both the translation of the state variables into policy space via the basis functions and the linear combination weights of the different basis functions.

An analogous formulation is used for a global information-assimilating policy:

$$
\begin{aligned}
BH_t^{glob} &= x_1 + x_2\beta_t^{loc} + x_3(\beta_t^{loc})^2 + x_4 srss_t^{loc} + x_5(srss_t^{loc})^2 \\
&\quad + x_6\beta_t^{ice} + x_7(\beta_t^{ice})^2 + x_8 srss_t^{ice} + x_9(srss_t^{ice})^2, \\
FH_t^{glob} &= x_{10} + x_{11}\beta_t^{loc} + x_{12}(\beta_t^{loc})^2 + x_{13} srss_t^{loc} + x_{14}(srss_t^{loc})^2 \\
&\quad + x_{15}\beta_t^{ice} + x_{16}(\beta_t^{ice})^2 + x_{17} srss_t^{ice} + x_{18}(srss_t^{ice})^2.
\end{aligned}
$$

The series of levee heightenings for a particular SOW (suppressing the policy notation) is then

$$
u_t = \begin{cases} 0, & BH_t \geq h_t^- - y_t \\ y_t - (h_t^- - BH_t) + FH_t, & BH_t < h_t^- - y_t. \end{cases}
$$

2.4 Objectives

The original objective in the Eijgenraam model[15] is to minimize the total discounted social cost (Equation (1)). Here we follow Garner and Keller[14] in disaggregating the investment cost and expected damages into two separate economic objectives:

$$\text{Objective 1}: \quad \min \frac{1}{\#\text{SOWs}} \sum_{i,t} I(h_{i,t}^{-}, u_{i,t}) e^{-\delta t}, \text{ and}$$
$$\text{Objective 2}: \quad \min \frac{1}{\#\text{SOWs}} \sum_{i,t} V_{i,t} e^{-\delta_1 t},$$

where i is the SOW index, t is the time index, and $I(h_{i,t}^{-}, u_{i,t})$ is given in Equation (2). The damage function S_t is modified from Equation (3) by replacing the analytic probability of levee overtopping with the numerical approximation by the proportion of SOWs in which the levee is overtopped in year t.

We add a third objective, to maximize the expected reliability of the policy is added as a third objective. We formalize this objective by minimizing the empirical exceedance probability, or the proportion of years across all SOWs in which the levee is overtopped:

$$\text{Objective 3}: \quad \min \frac{\sum_i \#\{\text{overtopping events}\}}{\#\text{sim years}},$$

where i is the SOW index. This objective reflects the interest in minimizing the number of flooding events, and is not affected by the timing of individual flood (unlike the economic objectives, which are discounted to reduce the negative impact of flooding events later in the simulation).

Multi-objective problem formulations can provide a transparent framework to analyze and understand the trade-offs associated with different objectives. While a single-objective formulation yields a single optimal (with respect to the particular weighting of the combined objectives) policy, multi-objective optimization yields a Pareto front of solutions. Pareto fronts consist of non-dominated solutions: no solution belonging to the Pareto front is outperformed by any other across all objectives. As a result, different solutions belonging to the Pareto front represent different trade-offs between objectives.

2.5 Optimization

One disadvantage of practical multi-objective optimization is the need for a numerical approximation to the true Pareto front. We find an approximate Pareto front using the Master-Slave Borg Multi-Objective Evolutionary Algorithm[32,33]. Evolutionary algorithms optimize target functions by proposing a set of input variable values, evaluating the objective value(s) corresponding to those inputs, and mutating the best-performing proposals to produce the next set of proposals. This process continues until a given number of function evaluations. We choose a limit of 100,000 function evaluations as a reasonable compromise between Pareto front improvement and computation time.

Both the proposal and mutation mechanisms of evolutionary algorithms require random number generation, and the results of a particular run are therefore sensitive to the random number seed. To find an overall set of non-dominated solutions, we repeat the Borg run five times with different seeds. The approximate Pareto fronts generated by each run were then combined to find an overall set of non-dominated solutions.

3 Results

Adding ice-sheet information can drastically improve the performance of levee-heightening strategies (Figure 2). If increased ice-sheet melting is observed, the inclusion of this information allows for levees to be heightened more aggressively in anticipation of accelerating sea-level rise.

The shown slices of the Pareto front for the two strategies start to visually diverge at approximately a 1/2000 exceedance probability, which is the protection standard for levee ring 16. We find little benefit in the assimilation of the ice-sheet contributions for lower reliability levels. This is perhaps intuitive, given that projected flood risk at those reliability levels is primarily driven by the distribution of surge intensities [2].

The minimum-cost solution for the global-information strategy outperforms the minimum-cost solution for the local-information strategy with respect to both expected damages and expected reliability. The local minimum-cost solution has a reliability of approximately 1/4500, as compared with 1/6000 for the solution which uses both local and global information. The overall economic value of information (across all of the SOWs used in optimization, which averages over RCPs 2.6, 4.5, 6.0, and 8.5), when comparing

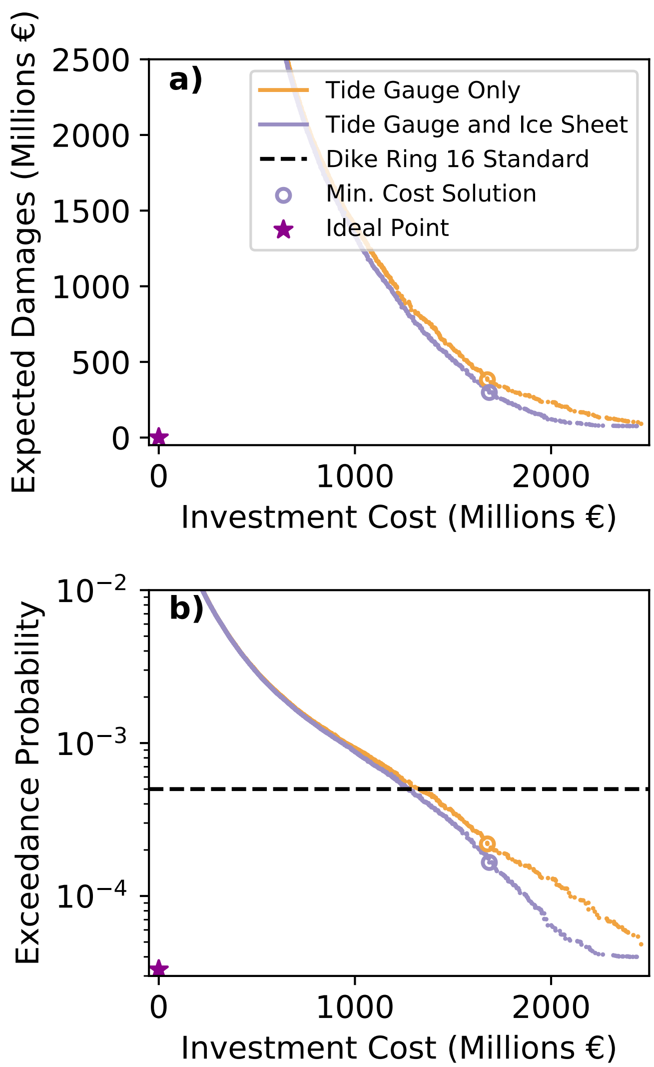

Figure 2: Non-dominated solutions for just the tide-gauge information (orange dots) and both tide-gauge and ice-sheet information (purple dots). Shown are the net present value of the economic objectives (a) and a combination of the reliability objective and the net present value of investment costs (b). The minimum-cost solution is the solution which minimizes the sum of the net present values of investments and damages over the optimization horizon.

Table 2: Relative value of information (VOI) associated with incorporating the ice-sheet contribution to sea-level rise in the flood defense strategy. For each representative concentration pathway (RCP), 100,000 states of the world were simulated. The minimum-cost policy was used for both the local-information and the global-information strategies.

RCP	**Relative VOI (%)**
2.6	2%
4.5	5%
6.0	5%
8.5	5%

minimum-cost solutions, is approximately 4%.

We re-analyze the minimum-cost solutions with respect to different RCPs to quantify how the economic value of information (VOI) changes with increased emissions (Table 2). In general (and perhaps unsurprisingly), higher-emissions trajectories made the ice sheet information more valuable, as the associated increase in global temperatures increase the probability of accelerated ice sheet disintegration within the considered time frame(12).

This re-analysis also let us look at the adaptiveness of the minimum-cost solutions over time. The local-information solution had a median freeboard height delta (the difference between the maximum over the time series for that SOW and the minimum) of 79 centimeters, while this median value was over a meter (108 centimeters) for the global information solution. For the buffer heights, the median delta for the local-information solution was 18 centimeters, compared to 22 centimeters for the global-information solution. These differences are much higher than those found by Garner and Keller(14), which we attribute to the different sea-level rise model and the non-stationary surge distributions. The primary driver of year-to-year variability for both levers in both information cases is the $\mathrm{srss}_t^{\mathrm{loc}}$ state variable (the correlations between this variable and the freeboard and buffer heights is largest), which tracks the volatility of the extreme water levels around the trendline.

4 Caveats

We use a simple model to analyze the impacts of ice-sheet observations on the performance of flood-risk management strategies. The model's simplicity allows for a relatively transparent analysis, but also requires several caveats. Here we discuss a few key caveats.

First, we only consider one levee-failure mechanism, namely overtopping. In reality, levees can fail due to other mechanisms, including piping [34]. As a result, we likely underestimate the costs of both damages and investments (due to levee breaches).

Second, we consider a representative setting for this analysis, rather than a particular case study. While levee ring 16 is not exposed to the coast, we use its economic parameters from the original Eijgenraam model for convenience. We combined this economic model with water-level dynamics calibrated using data from Delfzijl. As the relationship between Greenland and Antarctic ice-sheet melting and local sea-level rise rates depends on the particular location[13, 35], the extent to which these results generalize will be dependent on the strength of that relationship.

Third, as discussed in Section 2.2, we use a simple approach to model surge non-stationarity. It is not clear that temperature dependence is ideal for realistically representing future climate-related changes to extreme water level distributions, and other proxies (which might result in smaller surge distribution tails) could produce a lower expected value of information.

Fourth, we use a continuous policy formulation, in which the policy levers were adjusted each year as a function of the state variables. Moreover, we optimized policies with respect to their average performance across all possible futures. The decision-making process used by real-world coastal planners is typically aimed at defending against selected future scenarios, with more discrete mechanisms for adapting to changes in scenario likelihood[36]. While we incorporated ice-sheet observations as a continuous state variable, a scenario-based approach might use satellite images of collapsing ice sheets or a sharp increase in estimated ice-sheet melt rates to as a signpost to trigger a switch to a different adaptation strategy. Additionally, real policies might mix several different adaptation levers, including changing building codes to increase resilience and decrease damages[(37)].

Finally, observations of ice sheets may not provide an optimal balance between costs of observation and information value. Other, easier to obtain information signals about sea-level rise or other drives of changing extreme water levels may have a higher value of information. Our goal in this analysis was to focus on understanding how recent advances in ice-sheet science might benefit local planners.

5 Conclusions

This study illustrates the utility of sustained Earth observations to inform coastal flood defense strategies. These observation platforms already provide multiple value streams, including benefits to shipping, fishing, and recreation[38,39].

While the primary driver of adaptiveness of the policies identified in this study is the yearly variation in extreme surges (which is consistent with the results by Wong et al[12], accounting for ice sheet disintegration in this policy formulation yields better performance at similar investment levels.

Our analysis demonstrates the economic value of information concerning ice-sheet dynamics. Adaptive frameworks which naturally fit into this type of planning[40] rely on observable signposts to trigger changes in strategy. Sustained observations and scientific analyses of ice-sheet dynamics can serve as an important signpost, providing early warning signs about decision-relevant changes in sea levels.

References

1. Oddo, P. C. *et al.* Deep uncertainties in sea-level rise and storm surge projections: Implications for coastal flood risk management. *Risk Anal.* doi:`10.1111/risa.12888` (2017).

2. Wong, T. E. & Keller, K. Deep uncertainty surrounding coastal flood risk projections: A case study for New Orleans: Probabilistic projections of flood risk. *Earth's Future.* doi:`10.1002/eft2.255` (2017).

3. Wahl, T *et al.* Understanding extreme sea levels for broad-scale coastal impact and adaptation analysis. *Nat. Commun.* **8,** 16075 (2017).

4. Sweet, W. V. *et al. Global and regional sea level rise scenarios for the United States* tech. rep. NOS CO-OPS 083 (NOAA, 2017).

5. Lee, B. S., Haran, M. & Keller, K. Multidecadal scale detection time for potentially increasing Atlantic storm surges in a warming climate. *Geophys. Res. Lett.* **44,** 2017GL074606 (2017).

6. Langlois, R. N. & Cosgel, M. M. FRANK KNIGHT ON RISK, UNCERTAINTY, AND THE FIRM: a NEW INTERPRETATION. *Econ. Inq.* **31,** 456–465 (1993).

7. Walker, W. E., Haasnoot, M. & Kwakkel, J. H. Adapt or perish: a review of planning approaches for adaptation under deep uncertainty. *Sustain. Sci. Pract. Policy* **5,** 955–979 (2013).

8. Slangen, A. B. A. *et al.* The impact of uncertainties in ice sheet dynamics on Sea-Level allowances at tide gauge locations. *Journal of Marine Science and Engineering; Basel* **5,** 21 (2017).

9. Pollard, D., DeConto, R. M. & Alley, R. B. Potential Antarctic ice sheet retreat driven by hydrofracturing and ice cliff failure. *Earth Planet. Sci. Lett.* **412,** 112–121 (2015).

10. DeConto, R. M. & Pollard, D. Contribution of Antartica to past and future sea-level rise. *Nature* **531,** 591–597 (2016).

11. Haran, M., Chang, W., Keller, K., Nicholas, R. & Pollard, D. Statistics and the future of the Antarctic ice sheet. *Chance* **30,** 37–44 (2017).

12. Wong, T. E., Bakker, A. M. R. & Keller, K. Impacts of Antarctic fast dynamics on sea-level projections and coastal flood defense. *Climatic Change,* 1–13 (2017).

13. Forsberg, R., Sørensen, L. & Simonsen, S. in *Integrative Study of the Mean Sea Level and Its Components* (eds Cazenave, A., Champollion, N., Paul, F. & Benveniste, J.) 91–106 (Springer International Publishing, Cham, 2017). doi:10.1007/978-3-319-56490-6_5.

14. Garner, G. G. & Keller, K. Using direct policy search to identify robust strategies in adapting to uncertain sea-level rise and storm surge. *Environmental Modelling & Software* **107,** 96–104 (2018).

15. Eijgenraam, C. *et al.* Economically efficient standards to protect the netherlands against flooding. *Interfaces* **44,** 7–21 (2014).

16. Van Dantzig, D. Economic decision problems for flood prevention. *Econometrica* **24,** 276–287 (1956).

17. Eijgenraam, C., Brekelmans, R., den Hertog, D. & Roos, K. Flood prevention by optimal dike heightening. *Delft University of Technology, the Netherlands, Working Paper,* 1–17 (2012).

18. Wong, T. E. *et al.* BRICK v0.2, a simple, accessible, and transparent model framework for climate and regional sea-level projections. *Geoscientific Model Development* **10,** 2741–2760 (2017).

19. Coles, S. *An Introduction to Statistical Modeling of Extreme Values* (Springer-Verlag London, London, 2001).

20. Ceres, R. L., Forest, C. E. & Keller, K. Understanding the detectability of potential changes to the 100-year peak storm surge. *Clim. Change.* doi:`10.1007/s10584-017-2075-0` (2017).

21. *Rijkswaterstaat 2017* `http://live.waterbase.nl`. Accessed: 2017-12-16. 2017.

22. Menéndez, M. & Woodworth, P. L. Changes in extreme high water levels based on a quasi-global tide-gauge data set. *J. Geophys. Res.* **115,** 267 (2010).

23. Grinsted, A., Moore, J. C. & Jevrejeva, S. Projected Atlantic hurricane surge threat from rising temperatures. *Proc. Natl. Acad. Sci. U. S. A.* **110,** 5369–5373 (2013).

24. Watanabe, S. Asymptotic equivalence of Bayes cross validation and widely applicable information criterion in singular learning theory. *J. Mach. Learn. Res.* **11,** 3571–3594 (2010).

25. Gelman, A., Hwang, J. & Vehtari, A. Understanding predictive information criteria for Bayesian models. *Stat. Comput.* **24,** 997–1016 (2014).

26. Akaike, H. A new look at the statistical model identification. *IEEE Transactions on Automatic Control* **19,** 716–723 (1974).

27. Schwarz, G. Estimating the dimension of a model. *Ann. Stat.* **6,** 461–464 (1978).

28. Deisenroth, M. P., Neumann, G. & Peters, J. A survey on policy search for robotics. *Foundations and Trends® in Robotics* **2,** 1–142 (2013).

29. Giuliani, M., Castelletti, A., Pianosi, F., Mason, E. & Reed, P. M. Curses, tradeoffs, and scalable management: Advancing evolutionary multiobjective direct policy search to improve water reservoir operations. *Journal of Water Resources Planning and Management* **142,** 04015050 (2016).

30. Quinn, J. D., Reed, P. M. & Keller, K. Direct policy search for robust multi-objective management of deeply uncertain socio-ecological tipping points. *Environmental Modelling & Software* **92,** 125–141 (2017).

31. Van der Pol, T. D., van Ierland, E. C. & Weikard, H. P. Optimal dike investments under uncertainty and learning about increasing water levels. *Journal of Flood Risk Management* **7,** 308–318 (2014).

32. Hadka, D. & Reed, P. Borg: An Auto-Adaptive Many-Objective evolutionary computing framework. *Evol. Comput.* **21,** 1–30 (2012).

33. Hadka, D. & Reed, P. Large-scale parallelization of the borg multiobjective evolutionary algorithm to enhance the management of complex

environmental systems. *Environmental Modelling & Software* **69,** 353–369 (2015).

34. Vorogushyn, S, Merz, B & Apel, H. Development of dike fragility curves for piping and micro-instability breach mechanisms. *Nat. Hazards Earth Syst. Sci.* **9,** 1383–1401 (2009).

35. De Winter, R. C. *et al.* Impact of asymmetric uncertainties in ice sheet dynamics on regional sea level projections. *Nat. Hazards Earth Syst. Sci.* **17,** 2125–2141 (2017).

36. USACE. *Procedures to evaluate sea level change: Impacts, responses, and adaptation* tech. rep. ETL 1100-2-1 (USACE, 2014).

37. Aerts, J. C. J. *et al.* Evaluating flood resilience strategies for coastal megacities. *Science* **344,** 473–475 (2014).

38. Dumas, C. F. & Whitehead, J. C. The potential economic benefits of coastal ocean observing systems: The southeast Atlantic region. *Coast. Manage.* **36,** 146–164 (2008).

39. Weatherhead, E. C. *et al.* Designing the climate observing system of the future. *Earth's Future* **6,** 80–102 (2018).

40. Haasnoot, M., Kwakkel, J. H., Walker, W. E. & ter Maat, J. Dynamic adaptive policy pathways: A method for crafting robust decisions for a deeply uncertain world. *Glob. Environ. Change* **23,** 485–498 (2013).

41. Caldwell, P. C., Merrifield, M. A. & Thompson, P. R. *Sea level measured by tide gauges from global oceans — the Joint Archive for Sea Level holdings (NCEI Accession 0019568)* 2015. doi:10.7289/V5V40S7W.

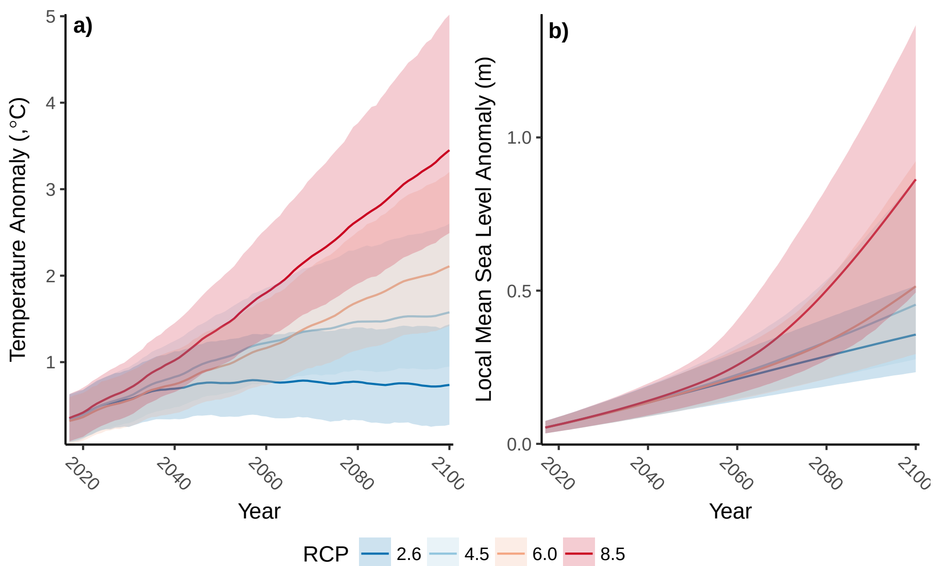

Figure S1: Global mean temperature (a)) and local mean sea level (at the Delfzijl tide gauge, b)) anomaly projections from BRICK. Anomalies are relative to the 2000 mean value. The lines are the mean projected values and the shaded regions are the 95% credible intervals.

GEV Parameter	**Prior Distribution**
Location Intercept (μ_0)	$\text{Gamma}(1.37, 0.0007)$
Location Temperature Coefficient (μ_1)	$N(37.45, 462.42)$
Scale (σ)	$\text{Gamma}(0.32, 0.0027)$
Shape (ξ)	$N(-0.16, 0.50)$

Table S1: Prior distributions for non-stationary GEV parameters used to model extreme water level residuals. The prior distributions were derived using data from the University of Hawaii Sea Level Center[(41)], based on the maximum-likelihood estimates for each tide gauge station within 35–60° N and -11–11° E that had at a record length of least 30 years. Parameters with infinite support were modeled using normal distributions fit to the maximum-likelihood estimates, while parameters with half-infinite support were modeled using gamma distributions.

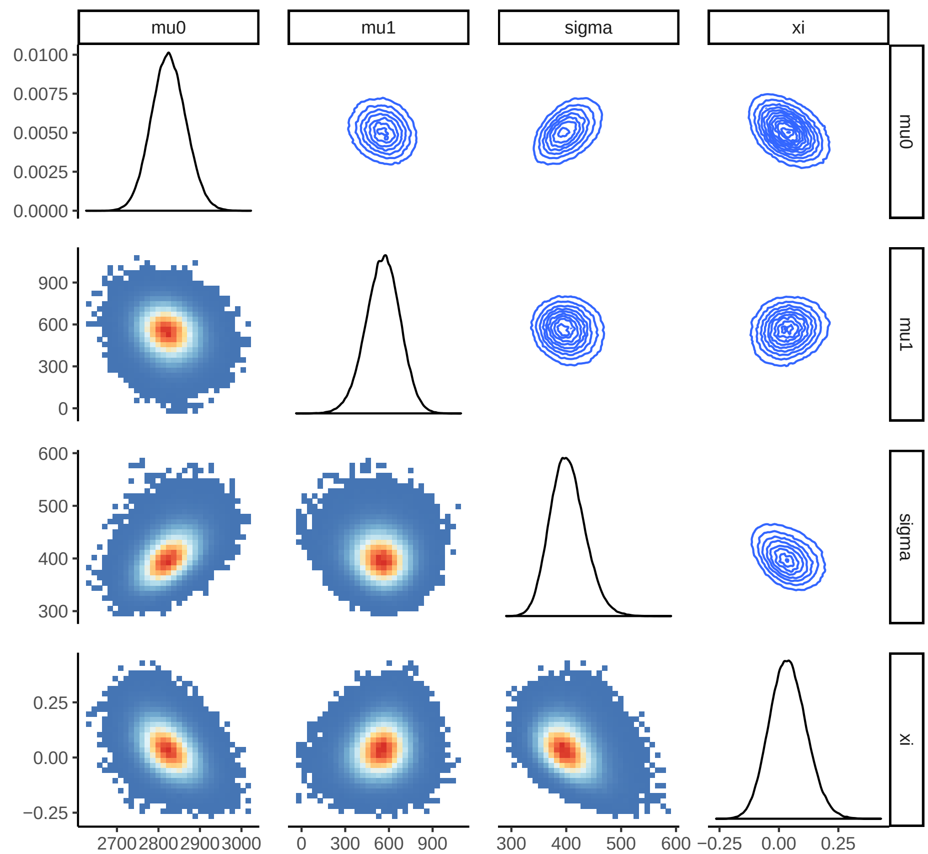

Figure S2: Pairs plot for the GEV posterior distribution. Marginal posterior distribution densities are along the diagonal, pairwise bins below the diagonal, and pairwise densities above the diagonal.